

JGR Solid Earth

RESEARCH ARTICLE

10.1029/2021JB022422

Key Points:

- An early-time solution was developed for pulse-decay measurements of ultratight rocks
- Gas compressibility and slippage effects are considered in the derivation
- The validity and efficiency of this model were verified through experimental measurements

Correspondence to:

M. Wang,
mrwang@tsinghua.edu.cn

Citation:

Wang, Y., Nolte, S., Gaus, G., Tian, Z., Amann-Hildenbrand, A., Krooss, B., & Wang, M. (2021). An early-time solution of pulse-decay method for permeability measurement of tight rocks. *Journal of Geophysical Research: Solid Earth*, 126, e2021JB022422. <https://doi.org/10.1029/2021JB022422>

Received 13 MAY 2021

Accepted 17 NOV 2021

Author Contributions:

Conceptualization: Moran Wang
Data curation: Steffen Nolte, Garri Gaus
Investigation: Yue Wang, Steffen Nolte, Zhiguo Tian, Moran Wang
Methodology: Yue Wang
Project Administration: Moran Wang
Software: Zhiguo Tian
Supervision: Bernhard Krooss, Moran Wang
Validation: Yue Wang
Writing – original draft: Yue Wang
Writing – review & editing: Steffen Nolte, Zhiguo Tian, Alexandra Amann-Hildenbrand, Bernhard Krooss, Moran Wang

An Early-Time Solution of Pulse-Decay Method for Permeability Measurement of Tight Rocks

Yue Wang¹, Steffen Nolte² , Garri Gaus² , Zhiguo Tian¹, Alexandra Amann-Hildenbrand², Bernhard Krooss² , and Moran Wang¹ 

¹Department of Engineering Mechanics, Tsinghua University, Beijing, China, ²Institute of Geology and Geochemistry of Petroleum and Coal, Energy and Mineral Resources Group (EMR), RWTH Aachen University, Aachen, Germany

Abstract This contribution presents an early-time solution for permeability evaluation in pulse-decay tests. A nonlinear governing equation for gas transport in the sample is derived considering the pressure dependence of gas compressibility and Klinkenberg slippage effect, and the early-time solution is obtained through the integral balance analysis. The permeability coefficient can be determined by the proposed solution through the pressure transients during the early-time stage of the tests, that is, before the upstream pressure pulse penetrates through the core sample and reaches the downstream side. To test the proposed solution, measurements were performed on a core sample of the Cretaceous Eagle Ford shale, Texas, USA, under different pore and confining pressures. Helium was used as the testing fluid to minimize the Joule-Thomson effect and adsorption. The experimental results show that the permeability coefficients obtained from this new solution agree well with those from the late-time solution, and prove our solution accurate and efficient for permeability evaluation. The present approach provides a good supplement to the pulse-decay method and is suitable for measurements of low-permeable rocks.

Plain Language Summary Unconventional natural gas has become an increasingly important energy source in recent years and has attracted active research and development accordingly. One key problem in unconventional natural gas reservoir exploitation is the determination of the viability of commercial production, where permeability is a critical parameter. The pulse-decay test is the most popular method of permeability measurement for low-permeable rocks. It requires analytical solutions to evaluate the permeability coefficient from pressure records. Most previous methods are based on late-time solutions that interpret the late-time pressure data and omit the information in the early-time stage. The early-time solution developed in this work interprets the early-stage pressure data and considers the variation of gas compressibility and the Klinkenberg slippage effect. The validity and efficiency of the proposed solution are testified by both numerical simulation and experimental measurements.

1. Introduction

Unconventional natural gas has become more and more important throughout the world. One key problem is the determination of the viability of commercial production, for which permeability is the critical parameter (Darabi et al., 2012; Liu et al., 2018; Wang et al., 2018; Zhao et al., 2020). However, due to the tightness of these rocks, permeability measurements using the steady state method are very time consuming (Heller & Zoback, 2013; Metwally & Sondergeld, 2011). One of the most widely used transient methods is the pulse-decay method (Brace et al., 1968; Gaus et al., 2019; Winhausen et al., 2021). In the typical pulse-decay tests, a cylindrical rock sample is installed in a flow cell connected to two reservoirs. At the initial stage, the sample is pressure-equilibrated at a defined pressure. Thereafter, a pressure pulse is applied in the upstream compartment and the resulting pressure decay is recorded with time. For tight rocks, the pulse-decay method has the advantages of efficiency (a steady state is not required to be reached) and accuracy (the measurement of pressure is more accurate than that of flux) (Akkutlu & Fathi, 2012; Yang et al., 2016). Different from the steady state method, where the permeability coefficient can be calculated directly through Darcy's law, the permeability coefficient in the pulse-decay method is determined by fitting the analytical solution to the measured pressure transients.

The first analytical solution was reported by Brace et al. (1968), who used the one-dimensional mass balance equation combined with Darcy's law to describe the pulse-decay process. A single exponential solution was obtained, which is, however, only valid when the reservoir volumes are much larger than the sample's pore volume.

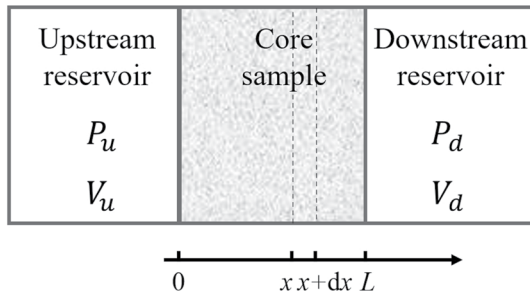


Figure 1. Scheme of a pulse-decay test. Upstream and downstream sides are indicated by subscripts u and d, respectively.

Later, Dicker and Smits (1988) removed the restriction on reservoir size and obtained a series solution that can be reduced to a single exponential form at the late-time stage. Jones (1997) further simplified Dicker and Smits' expression by introducing a mass flow correction factor and proposed a strategy to reduce the test time of pulse-decay experiments. Solutions with explicit consideration of the adsorption effect were developed by Cui et al. (2009). Han et al. (2018) analyzed the pulse-decay process for dual-porosity samples.

The above solutions are all “late-time solutions” (Sander et al., 2017) that omit the information contained at the early-time stage, the consideration of which may help to improve time efficiency and accuracy of the measurements. Hsieh et al. (1981) proposed an early-time solution obtained by Laplace transformation. However, this solution is not convenient for practical application because of the complexity of the complementary error function

(erfc) involved and the lack of a cooperating method to determine the duration of the early-time stage. In their derivation, Hsieh et al. assumed constant fluid compressibility (usually the value at the mean fluid pressure), which works well when liquids are used as test media but maybe invalid when gases are used in the measurements (Feng et al., 2018; Liang et al., 2001; Wu et al., 2020).

In this study, an early-time solution has been developed for the interpretation of early-time pressure data in pulse-decay tests. A nonlinear governing equation for gas transport in the sample is derived considering gas compressibility and the Klinkenberg slippage effect, and the early-time solution is obtained by the integral method. The only undetermined constant in the final expression for apparent permeability was obtained from numerical simulation. Both numerical simulation and experimental measurement were performed to test the proposed solution.

2. Physical and Mathematical Models

2.1. Derivation of the Governing Equation

In a typical pulse-decay test, a rock sample is placed in a measuring cell connected to two gas reservoirs. Here we consider a small control volume between x and $x + dx$, as shown in Figure 1. Assuming that Darcy's law is valid (i.e., we have a linear relationship between volume flux and pressure gradient) in the control volume, the mass flow q (kg s^{-1}) along the x axis is,

$$q = -\rho \frac{k_{app} A}{\mu} \frac{dP}{dx} \quad (1)$$

Here ρ is the gas density (kg m^{-3}), k_{app} the apparent permeability coefficient (m^2), A the cross-section area of the sample (m^2), μ the dynamic viscosity of the gas (Pa s), and P is the gas pressure (Pa).

The mass change of gas in the control volume $\phi A dx$ per unit time is equal to the net flow:

$$\frac{d}{dt}(\rho A \phi dx) = dq \quad (2)$$

Here ϕ is the porosity of the sample.

Substituting Equation 1 into Equation 2 yields the governing equation of pulse-decay tests at constant temperature:

$$\frac{\partial}{\partial t}(\rho A \phi) = \frac{\partial}{\partial x} \left(\rho \frac{k_{app} A}{\mu} \frac{\partial P}{\partial x} \right) \quad (3)$$

The density of the gas is related to its pressure through the equation of state,

$$\rho = \frac{M}{ZRT} P \quad (4)$$

where M is the molar mass of the test gas (kg mol^{-1}), Z the compressibility factor, R the gas constant ($8.314 \text{ J mol}^{-1} \text{ K}^{-1}$), and T the absolute temperature (K). In the experimental part of this study, helium was

used as testing fluid. Within the pressure range of the measurements (0.1–10 MPa), the compressibility factor Z for helium is very close to the value of one, with an error smaller than 5% (McCarty & Arp, 1990; Nolte et al., 2021). Thus, the density ρ in Equation 3 could be replaced by the pressure P when multiplying both sides of Equation 3 by M/ZRT . We also have the expression for the compressibility of gas density as a function of pressure:

$$\beta_\rho = \frac{\partial \ln \rho}{\partial P} = \frac{1}{P} - \frac{\partial \ln Z}{\partial P} \approx \frac{1}{P} \quad (5)$$

Substituting Equations 4 and 5 into Equation 3, we get:

$$\frac{\partial}{\partial t}(P\phi) = \frac{\partial}{\partial x} \left(\frac{k_{app}}{\beta_\rho \mu} \frac{\partial P}{\partial x} \right) \quad (6)$$

From experimental observations, many models have been proposed to account for the dependence of apparent permeability on pressure due to gas slippage. The widely used Klinkenberg formula (Klinkenberg, 1941) is adopted in this study:

$$k_{app}(P) = k_{int} \left(1 + \frac{b_s}{P} \right) \quad (7)$$

where k_{int} is the intrinsic permeability coefficient (m^2) and b_s is the Klinkenberg slippage factor (Pa).

If we assume the compressibility and viscosity of the gas, as well as the apparent permeability and porosity of the sample, are all constants and replace them with their values at the mean pore pressure (e.g., $\beta_\rho = \beta_\rho(P_{mean})$, and $k_{app} = k_{app}(P_{mean})$, $P_{mean} = (P_u(0) + P_d(0))/2$), Equation 6 will be reduced to the linear form that was obtained by Brace et al. (1968). However, during the pulse-decay test, the pressure within the sample is not uniform, causing these pressure-dependent parameters to vary along the length of the sample. To determine whether one parameter can be approximated as constant, the relative change in its value caused by pressure variation (or nonuniformity) needs to be estimated:

$$\Delta_r X = \frac{\Delta X}{X} = \frac{1}{X} \frac{\partial X}{\partial P} \Delta P = \beta_X \Delta P \quad (8)$$

where $\Delta_r X$ denotes the relative change of parameter X , ΔP the pressure difference in the pulse-decay test (Pa), and $\beta_X = \partial \ln X / \partial P$ is the pressure sensitivity of parameter X (Pa^{-1}). Strictly speaking, the gas compressibility, gas viscosity, sample porosity, intrinsic permeability, and Klinkenberg slippage factor are effective pressure-dependent, so the relative changes in their values need to be evaluated (i.e., $X = \beta_\rho, \mu, \phi, k_{int}$ or b_s). As shown in Equation 5, the gas compressibility β_ρ is equal to the reciprocal of pressure, and thus we have $\Delta_r \beta_\rho = -\Delta_r P = -\beta_\rho \Delta P$.

In pulse-decay tests, the initial pressure difference between two ends of the sample can be on the order of megapascals (i.e., $\Delta P = 10^6$ MPa) (Fedor et al., 2008; Feng & Pandey, 2017). Previous researches show that for the permeability measurements on shale matrix samples, the compressibility of gas density β_ρ is of the order of 10^7 – 10^5 Pa^{-1} , and those of gas viscosity, sample porosity, intrinsic permeability, and Klinkenberg slippage factor ($\beta_\mu, \beta_\phi, \beta_{k_{int}}, \beta_{b_s}$) are of the order of 10^{-9} to 10^{-8} Pa^{-1} (Chalmers et al., 2012; Dong et al., 2010; Fink et al., 2017; Senger et al., 2018; Sun et al., 2020). Therefore, $\Delta_r \beta_\rho$ is of the order of 10^{-1} to 10^1 , while the relative changes of the other four parameters ($\Delta_r \mu, \Delta_r \phi, \Delta_r k_{int}, \Delta_r b_s$) are of the order of 10^{-3} to 10^{-2} , which are small enough and can be ignored safely. Therefore, only the pressure dependence of β_ρ is considered in the following derivation. The intrinsic permeability k_{int} , Klinkenberg slippage factor b_s , and porosity ϕ of the sample, and the viscosity μ of the gas are regarded as constant.

With all the considerations above, Equation 3 simplifies to

$$\frac{\partial P}{\partial t} = \frac{1}{\mu \phi} \frac{\partial}{\partial x} \left(\frac{k_{app}}{\beta_\rho} \frac{\partial P}{\partial x} \right) \quad (9)$$

The pressure dependence of the apparent permeability coefficient k_{app} due to the Klinkenberg slippage effect is accounted for by Equation 7.

Substituting the expressions for β_p and k_{app} , Equations 5 and 7, into Equation 9, we have the final form of the governing equation:

$$\frac{\partial P}{\partial t} = \frac{k_{int}}{\mu\phi} \frac{\partial}{\partial x} \left((P + b_s) \frac{\partial P}{\partial x} \right) \quad (10)$$

which is nonlinear because we take the gas compressibility and the apparent permeability as pressure-dependent. The nonlinearity may be omitted in the late-time stage of the pulse-decay tests where the pressure difference ΔP in Equation 8 becomes small. However, in the early-time stage of the pulse-decay tests with a relatively large pressure difference (Feng et al., 2017; Wang et al., 2015), nonlinearity plays an important role. Equation 10 is the starting point of the current work.

Following a similar procedure, the boundary conditions at the two ends of the sample are obtained, which are also nonlinear:

$$\left. \frac{\partial P}{\partial t} \right|_{x=0} = \frac{k_{int}A}{\mu V_u} (P + b_s) \left. \frac{\partial P}{\partial x} \right|_{x=0} \quad (11)$$

$$\left. \frac{\partial P}{\partial t} \right|_{x=L} = -\frac{k_{int}A}{\mu V_d} (P + b_s) \left. \frac{\partial P}{\partial x} \right|_{x=L} \quad (12)$$

Here L is the length of the cylindrical sample (m), V_u and V_d are the volumes of the upstream and downstream reservoirs (m^3), respectively.

The initial conditions are given by:

$$P(x, 0) = \begin{cases} P_u(0), & x = 0 \\ P_d(0), & 0 < x \leq L \end{cases} \quad (13)$$

where $P_u(0)$ and $P_d(0)$ are the initial pressure values at upstream and downstream (Pa), respectively.

2.2. Model for Permeability Evaluation

For ease of derivation, the following dimensionless variables with subscript D are defined,

$$x_D = \frac{x}{L}, t_D = \frac{(P_{mean} + b_s)k_{int}t}{\mu\phi L^2}, P_D = \frac{P + b_s}{P_{mean} + b_s}, a = \frac{LA\phi}{V_u}, b = \frac{LA\phi}{V_d}, c = \frac{P_u(0) - P_d(0)}{P_u(0) + P_d(0) + 2b_s} \quad (14)$$

where x_D , t_D , P_D represent the dimensionless counterparts of x , t , P , respectively, $P_{mean} = (P_u(0) + P_d(0))/2$ the mean pore pressure, and a , b , c represent the upstream volume ratio, downstream volume ratio, and dimensionless pulse size (dimensionless initial pressure difference), respectively.

With these dimensionless variables, the governing Equation 10 can be rewritten as:

$$\frac{\partial P_D}{\partial t_D} = \frac{\partial}{\partial x_D} \left(P_D \frac{\partial P_D}{\partial x_D} \right) \quad (15)$$

and the dimensionless boundary and initial conditions are given by:

$$\left. \frac{\partial P_D}{\partial t_D} \right|_{x_D=0} = a P_D \left. \frac{\partial P_D}{\partial x_D} \right|_{x_D=0} \quad (16)$$

$$\left. \frac{\partial P_D}{\partial t_D} \right|_{x_D=1} = -b P_D \left. \frac{\partial P_D}{\partial x_D} \right|_{x_D=1} \quad (17)$$

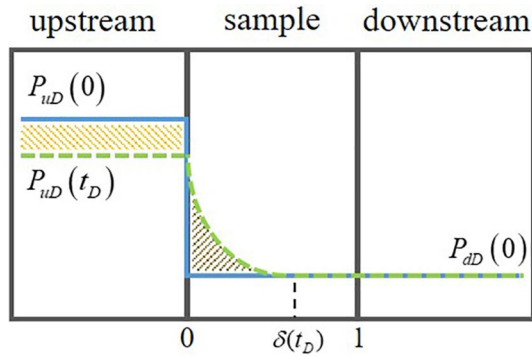


Figure 2. Scheme for the penetration depth $\delta(t_D)$. The pressure distributions within the setup at the beginning and instant t_D are represented by the blue solid line and the green dashed line, respectively. The penetration depth $\delta(t_D)$ denotes upstream pressure propagation front at instant t_D . The two shaded parts represent the mass of gas leaving the upstream reservoir and that of gas entering the sample, respectively.

$$P_D(x_D, 0) = \begin{cases} P_{uD}(0) = 1 + c, & x_D = 0 \\ P_{dD}(0) = 1 - c, & 0 < x_D \leq 1 \end{cases} \quad (18)$$

Getting an analytic solution to the nonlinear problem is usually impossible, so some approximations have to be introduced. In this study, we adopted the integral method (Özişik, 1989) to account for the early-time stage of the pulse-decay test, which is an approximation method first proposed by von Karman in the study of boundary layer momentum equations (Schlichting & Gersten, 2016) and is now widely used in the fields of fluid dynamics and heat conduction. This method is straightforward and applicable to both linear and nonlinear problems. Despite the approximate nature, the accuracy of the integral method is high enough for practical purposes (Hahn & Özisik, 2012).

The application of the integration method is generally divided into two steps. The first one is to introduce a phenomenological region, over which the governing equation is integrated to eliminate the spatial derivative, and the second one is to find an approximate solution that satisfies the integrated

equation. In the pulse-decay test of tight rocks, it is observed that when the pressure pulse is applied on the upstream side, the pressure on the downstream side increases only after a delay. The delay represents the time in which the gas penetrates from upstream to downstream through the sample and fills the interconnected pore volume. Inspired by such observation and the thermal layer concept in heat conduction (Hahn & Özisik, 2012), we introduce the penetration depth $\delta(t_D)$ to describe the length of the domain of influence of the pressure pulse at instant t_D . As shown in Figure 2, $\delta(t_D)$ denotes the position of the upstream pressure propagation front. According to this definition, at instant t_D , the region $0 \leq x_D \leq \delta(t_D)$ has been affected by the pressure pulse, while the region $\delta(t_D) \leq x_D \leq 1$ is unaffected and remains the initial pressure $P_d(0)$. Thus, we have:

$$P_D|_{x_D \geq \delta(t_D)} = P_{dD}(0) \quad \text{and} \quad \left. \frac{\partial P_D}{\partial x_D} \right|_{x_D \geq \delta(t_D)} = 0 \quad (19)$$

Then Equation 10 is integrated with respect to the space variable from $x_D = 0$ to $x_D = \delta(t_D)$:

$$P_D \left. \frac{\partial P_D}{\partial x_D} \right|_{x_D=0}^{x_D=\delta(t_D)} = \int_0^{\delta(t_D)} \frac{\partial P_D}{\partial t_D} dx_D \quad (20)$$

where the right-hand side can be rearranged with Leibniz's rule:

$$\int_0^{\delta(t_D)} \frac{\partial P_D}{\partial t_D} dx_D = \frac{d}{dt_D} \left(\int_0^{\delta(t_D)} P_D dx_D \right) - P_D|_{x_D=\delta(t_D)} \frac{d\delta}{dt_D} \quad (21)$$

Substituting Equations 19 and 21 into Equation 20, we have

$$-P_D \left. \frac{\partial P_D}{\partial x_D} \right|_{x_D=0} = \frac{d}{dt_D} [\theta - P_{dD}(0)\delta(t_D)] \quad (22)$$

where $\theta = \int_0^{\delta(t_D)} P_D dx_D$ represents the gas storage in the sample. Equation 22 is usually called the *balance integral* (Goodman, 1958) in heat conduction theory. Combining the balance integral and upstream boundary condition, we have:

$$\frac{d}{dt_D} [\theta - P_{dD}(0)\delta(t_D)] = -\frac{1}{a} \frac{dP_{uD}}{dt_D} \quad (23)$$

where the left-hand and right-hand sides represent the mass flow rate in the sample and upstream reservoir, respectively. Equation 23 is actually the mass conservation equation at the early-time stage of the pulse-decay test. It accounts for the fact that the mass of gas leaving the upstream reservoir equals the mass increase in the core

sample because when the pressure pulse from the upstream has not penetrated through the whole sample, there is no mass flux at the downstream interface.

An analytic model of the pressure profile across the penetration depth has to be adopted to make the calculation of θ possible. Any approximation or assumption could be an option, such as exponential or power functions (Faracas & Woods, 2007). Considering the complexity of mathematics and the consequent solution process, here we propose the penetration depth increase with the square root of the dimensionless time,

$$\delta(t_D) = m\sqrt{t_D} \quad (24)$$

where m is a constant. Inspired by the previous works on the pressure profile (Fabre & Hristov, 2016; Goodman, 1958; Mitchell & Myers, 2010), we assume a power function with an exponent n (see Equation 25) to describe the pressure profile within the penetration depth:

$$P_D(x_D, t_D) = [P_{uD}(t_D) - P_{dD}(0)] \left(1 - \frac{x_D}{\delta}\right)^n + P_{dD}(0), \quad 0 < x_D \leq \delta(t_D) \quad (25)$$

Substituting the pressure profile into Equation 23, we obtain the following equation:

$$\frac{d}{dt_D} \left[\frac{m}{n+1} (P_{uD}(t_D) - P_{dD}(0)) \sqrt{t_D} \right] = -\frac{1}{a} \frac{dP_{uD}}{dt_D} \quad (26)$$

Rearranging Equation (26) yields,

$$\frac{d}{dt_D} \left[\frac{m}{n+1} (P_{uD}(t_D) - P_{dD}(0)) \sqrt{t_D} + \frac{1}{a} P_{uD}(t_D) \right] = 0 \quad (27)$$

which means the value of the terms inside the square bracket is constant over time. Thus, if we choose two different instants (t_i, t_j) at the early-time stage, the corresponding terms inside the square bracket should be equal:

$$\begin{aligned} \frac{m}{n+1} (P_u(t_i) - P_d(0)) \sqrt{\frac{(P_{mean} + b_s) k_{int}}{\mu \phi L^2} t_i} + \frac{1}{a} P_u(t_i) \\ = \frac{m}{n+1} (P_u(t_j) - P_d(0)) \sqrt{\frac{(P_{mean} + b_s) k_{int}}{\mu \phi L^2} t_j} + \frac{1}{a} P_u(t_j) \end{aligned} \quad (28)$$

where the dimensionless variables have been transformed into the dimensional form.

By rearranging Equation 28, we obtain the expression for apparent permeability at the mean pore pressure:

$$k_{app}(P_{mean})_{(t_i, t_j)} = k_{int} \left(1 + \frac{b_s}{P_{mean}}\right) = \frac{1}{a^2} \left(\frac{n+1}{m}\right)^2 \frac{\mu \phi L^2}{P_{mean}} \left(\frac{P_u(t_i) - P_u(t_j)}{(P_u(t_i) - P_d(0)) \sqrt{t_i} - (P_u(t_j) - P_d(0)) \sqrt{t_j}} \right)^2 \quad (29)$$

where the subscripts (t_i, t_j) denote the two instants used for permeability evaluation. In addition to the parameters of the sample and testing gas, only the upstream pressure transients are involved here.

Equation 29 is the main result of this study, and it shows that if the value of $m/(n+1)$ is known, the apparent permeability $k_{app}(P_{mean})$ can be evaluated through the upstream pressure at different instants. The numerical results show that $m/(n+1) \approx 1.2$ and the validity of Equation 29 was tested by both numerical simulation and experimental measurements, as shown in the following section.

2.3. How to Use the Proposed Model

In the pulse-decay tests, after the application of the pressure pulse, the upstream pressure is recorded over time, and the corresponding instants are denoted by order as $t_0 < t_1 < t_2 < \dots$. Unlike the other late-time solutions that use the pressure transients in the late-time stage to evaluate the permeability coefficients, the proposed solution only needs the upstream pressure data at the early-time stage.

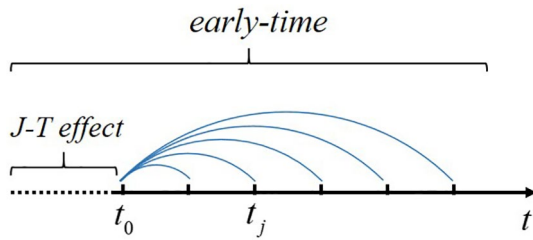


Figure 3. One way to select t_i and t_j in Equations 29 and 30, $(t_i, t_j) = (t_0, t_j), j = 1, 2, 3, \dots$. The data in a short period ($t < t_0$) at the beginning of the test is omitted to avoid the influence of the Joule-Thomson effect.

Theoretically, the upstream pressure transients at just two instants are enough to give the permeability value by Equation 29, and the instants t_i and t_j can be selected freely, as long as they are in the early-time stage of the pulse-decay test. However, in practice, due to the random error in pressure recording, the permeability value calculated through the pressure transients at just two instants may be inaccurate. The random error can be minimized by selecting a series of different (t_i, t_j) to calculate corresponding permeability values $k_{app}(P_{mean})_{(t_i, t_j)}$ and then take the average, that is,

$$k_{app}(P_{mean}) = \frac{1}{N} \sum_{(i,j)} k_{app}(P_{mean})_{(t_i, t_j)} \quad (30)$$

where N is the number of the selected (t_i, t_j) .

There are many ways to select (t_i, t_j) , and here we give one possible choice. As shown in Figure 3, we fix $t_i = t_0$, and then gradually increase t_j , that is, $(t_i, t_j) = (t_0, t_j), j = 1, 2, 3, \dots$.

The t_i and t_j in Equations 29 and 30 are required to be at the early-time stage of the pulse-decay test, so a practical way to determine the early-time stage is necessary. Here we take $(t_i, t_j) = (t_0, t_j)$. The numerical simulation in Section 3 shows that $(n + 1)/m$ is constant at the early-time stage (see Figure 6), so a horizontal line should be obtained if we plot the calculated permeability coefficient $k_{app}(P_{mean})_{(t_0, t_j)}$ against t_j when t_j is in the early-time stage. However, as t_j increases and goes beyond the early-time stage, the calculated permeability will deviate from the horizontal line, and such derivation can be used as an end criterion of the early-time stage.

The thermodynamics of gas has also been examined during this process. After the pressure pulse, the upstream gas pressure changes very rapidly. A sharp pressure change will induce a temperature change, which is known as the Joule-Thomson effect. The temperature change resulting from the unit pressure change is quantified by the Joule-Thomson coefficient ($\mu_{JT}(\text{K} \cdot \text{MPa}^{-1})$), which varies with the type, temperature, and pressure of the gas. The Joule-Thomson coefficient for an ideal gas is always zero, while those for real gases are not. In the derivation of the proposed model, the Joule-Thomson effect is ignored. However, this effect can be observed in experiments and needs special treatment.

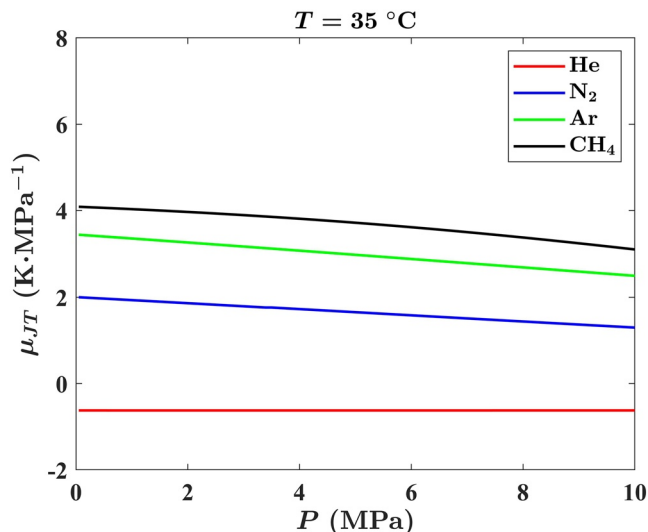


Figure 4. The Joule-Thomson coefficients of the gases commonly used in pulse-decay tests (data from NIST; <https://webbook.nist.gov/chemistry/liquid/>).

To minimize the influence of the Joule-Thomson effect, we chose helium as the testing fluid and used a thermal bath to keep the whole setup in temperature equilibrium. Helium was selected because it deviates only a little from an ideal gas and thus exhibits only a small Joule-Thomson coefficient. Besides, the choice of helium also helps to reduce the influence of adsorption. As shown in Figure 4, the Joule-Thomson coefficients of helium are much smaller than those of other gases (N_2 , Ar , CH_4), within the pressure range (0.1–10 MPa) of our experiments and at 35°C (308.15 K). For helium, a pressure change of 1 MPa will only cause a temperature decrease of about 0.6 K, which is less than 0.2% of the absolute temperature (308.15 K).

Therefore, for helium as the testing fluid, the temperature change caused by the Joule-Thomson effect will be small and will decline over several seconds if the setup is well thermostated (Hannon, 2020; Jia et al., 2020). To further eliminate the influence of the Joule-Thomson effect, we only use the pressure data starting from 20 s after the application of the pressure pulse (i.e., $t_0 \geq 20\text{s}$).

To illustrate the use of the proposed solution, we summarize the involved steps:

1. Equilibrate the whole setup at the desired pressure
2. Apply a pressure pulse to the upstream reservoir and then record the variations of $P_u(t)$ and $P_d(t)$, and denote the corresponding instants as $t_0 < t_1 < t_2 < \dots$

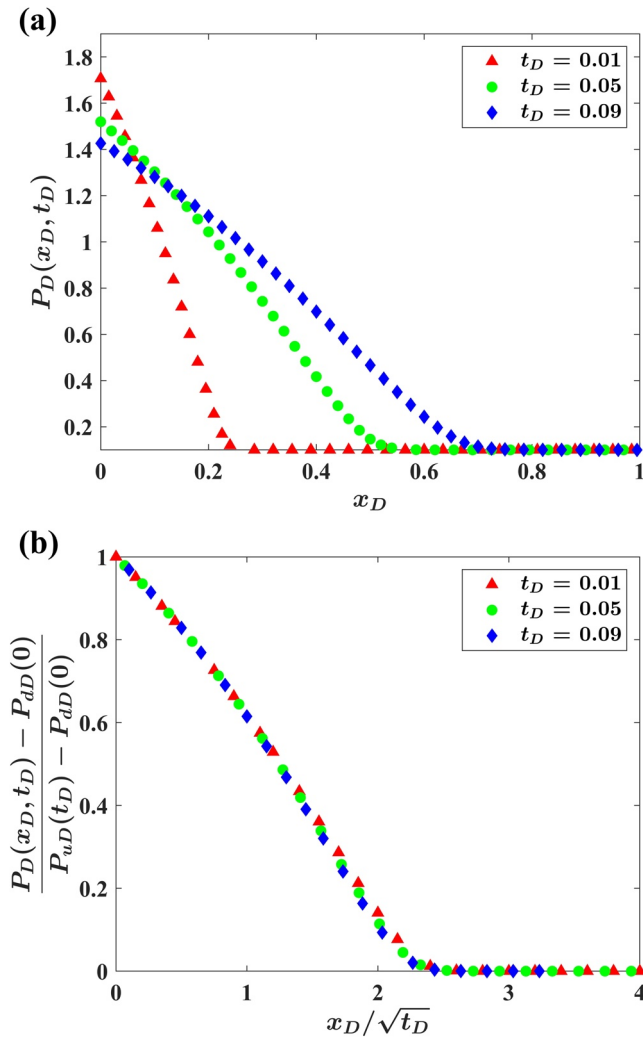


Figure 5. The numerical simulation results for pressure profile within the sample ($a = b = 1, c = 0.9$). (a) The pressure distribution at different instants. (b) The normalized pressure distribution in normalized spatial coordinates.

3. To avoid the Joule-Thomson effect, helium is taken as the testing fluid, and only the pressure data twenty seconds after the pulse is used ($t_0 \geq 20s$)
4. Choose a series of instants (t_i, t_j) at the early-time stage (e.g., $(t_i, t_j) = (t_0, t_j), j = 1, 2, 3, \dots$), and use the early-time pressure transients with Equations 29 and 30 to evaluate the apparent permeability
5. Optional: use late-time pressure data to evaluate the apparent permeability with the existing late-time solutions

3. Model Verifications

As outlined in detail in Section 2, some assumptions were introduced in the development of the proposed model for the evaluation of apparent permeability. These assumptions inevitably bring uncertainties into the final expression (29) and their rationality needs verification. In this section, the validity and accuracy of the model are justified by numerical simulation.

The finite difference method is adopted in the simulation. The dimensionless governing Equation 15 is discretized by the Crank-Nicolson scheme and its nonlinearity is coped with by Richtmyer's linearization method (Richtmyer & Morton, 1994). Since the porosity of the tight rocks is generally small, the reservoir volume in pulse-decay tests is usually larger than the pore volume of the sample, so the pore volume to reservoir volume ratios is set to be less than one in the simulation ($a, b \leq 1$). The simulation results of the pressure variations are used as input in the following analysis.

We first check the rationality of the selected pressure profile. By rearranging Equation 25, we have:

$$\frac{P_D(x_D, t_D) - P_{dD}(0)}{P_{uD}(t_D) - P_{dD}(0)} = \left(1 - \frac{1}{m} \frac{x_D}{\sqrt{t_D}}\right)^n \quad (31)$$

where the left-hand side is the pressure distribution normalized to the instantaneous pressure difference between the two ends of the sample, and the right-hand side is a function depending solely on the spatial coordinate normalized to the square root of time. Equation 31 indicates that the normalized pressure distributions at different instants should converge to the same curve in the normalized spatial coordinate.

The pressure distribution changes for different instants in the simulation (see Figure 5a). During the early-time stage, the upstream pulse propagation front has not penetrated through the whole sample, and the upstream pressure keeps decreasing while the downstream pressure remains constant. As time increases, the area affected by the upstream pressure pulse expands, that is, $\delta(t_D)$ increases. Consistent with Equation 31, the normalized pressure distributions at different instants converge to the same curve in the normalized spatial coordinate (see Figure 5b), which justifies our selection of the pressure profile.

After verifying the selected pressure profile, we also need to determine the value of $m/(n+1)$ that appears in the expression for permeability evaluation. To avoid the influence of the Joule-Thomson effect in the experiments, t_i and t_j in Equation 29 are required to be larger than twenty seconds. However, this requirement can be relaxed when dealing with the simulation results, because there is no Joule-Thomson effect in the simulation. As we set $t_i = 0, t_j = t$, Equation 29 transforms into:

$$\frac{1}{a} P_u(0) = \frac{m}{n+1} (P_u(t) - P_d(0)) \sqrt{\frac{(P_{mean} + b_s)k_{int}}{\mu\phi L^2} t} + \frac{1}{a} P_u(t) \quad (32)$$

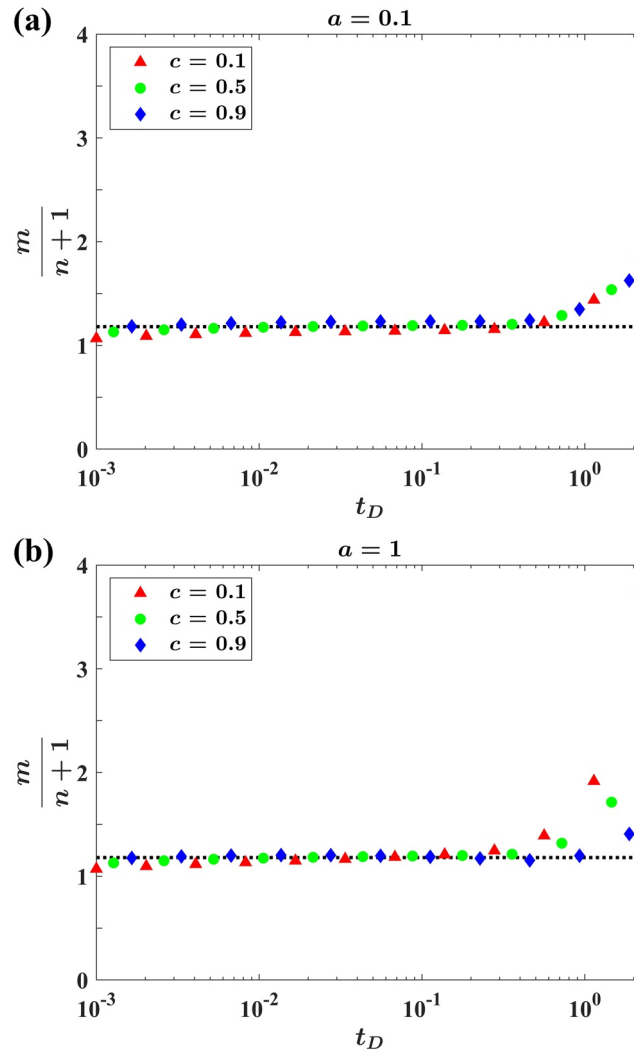


Figure 6. Variations of $m/(n + 1)$ with time and different initial pressure pulse c . The horizontal lines represent $m/(n + 1) = 1.2$. (a) $a = b = 0.1$ (b) $a = b = 1$.

By rearranging Equation 32 and rewriting it with the dimensional variables, we get an expression for the unknown prefactor $m/(n + 1)$:

$$\frac{m}{n + 1} = \frac{1}{a\sqrt{t_D}} \frac{P_{uD}(0) - P_{uD}(t_D)}{P_{uD}(t_D) - P_{uD}(0)} \quad (33)$$

The simulated pressure data are substituted into the right-hand side of Equation 33 to calculate $m/(n + 1)$ and the results are shown in Figure 6. Regardless of the volume ratio a and the dimensionless pulse size c , $m/(n + 1)$ remains constant (≈ 1.2 , marked by the horizontal lines) at the early-time stage of the pulse-decay test, as we assumed in the derivation (Section 2). It should be pointed out that the value of $m/(n + 1)$ obtained here is based on the governing Equation 10. The value of $m/(n + 1)$ might vary when the form of the governing equation changes, for example, the testing gas changes from helium (inert) to methane (adsorptive).

As time increases and goes beyond the early-time stage, $m/(n + 1)$ deviates from the horizontal line and is no longer constant. Consequently, if we substitute the pressure data beyond the early-time stage into Equation 29 and still take $m/(n + 1) = 1.2$, the permeability values obtained will deviate from those calculated with early-time pressure data. This deviation helps to determine the end of the early-time stage of the measurement.

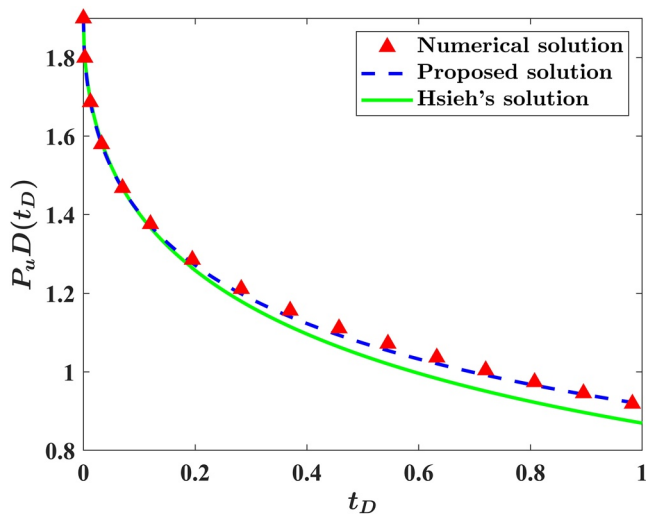


Figure 7. The upstream pressure transients given by numerical simulation, the proposed solution and Hsieh's solution. Here we set $a = b = 1$, $c = 0.9$, $m/(n + 1) = 1.2$.

Finally, we give a comparison between Hsieh's early-time solution (Hsieh et al., 1981) and the proposed solution. Hsieh's solution is in a complex form involving an exponential function and a complementary error function:

$$P_{uD}(t_D) = [P_{uD}(0) - P_{dD}(0)]e^{a^2 t_D} \operatorname{erfc}(a\sqrt{t_D}) + P_{dD}(0) \quad (34)$$

and the proposed solution can be rewritten from Equation 33 as follows:

$$P_{uD}(t_D) = \frac{P_{uD}(0) - P_{dD}(0)}{\frac{m}{n+1} a \sqrt{t_D} + 1} + P_{dD}(0) \quad (35)$$

which is in a much simpler form than Hsieh's solution.

The upstream pressure variations predicted by the proposed solution and Hsieh's solution are compared in Figure 7 and the simulated pressure data are also presented as a benchmark. Since the nonlinear effects caused by the pressure dependence of the gas compressibility and apparent permeability are not considered, Hsieh's solution gives the underestimated results. A good agreement is found between the proposed solution and the numerical solution, which proves that our solution can well capture the nonlinear effects.

4. Experimental Measurements

In this section, we apply the proposed method to interpret gas pulse-decay tests performed on a core sample of the Cretaceous Eagle Ford shale, Texas, USA. Helium was used as the testing fluid to minimize the influence of the Joule-Thomson effect and gas adsorption on the pore walls. The scheme of the experimental setup is shown in Figure 8. A detailed description of the experimental setup can be found in our earlier publications (Gaus et al., 2019; Ghanizadeh et al., 2014; Nolte et al., 2021). The experimental protocol is briefly outlined as follows:

1. The core sample was dried at 105 °C for at least 24 hr until weight constancy was achieved
2. The core sample was put into the core holder, with two porous steel discs connected to its two ends to make the inlet and outlet flow uniform. The sample was separated from the confining fluid by a double-layer sleeve, and a confining pressure was applied to mimic reservoir conditions. An oven was used to keep the setup in thermal equilibrium (35 ± 0.3 °C)
3. With valves 1, 2, and 3 open and valve 4 closed (see Figure 8), the core and two reservoirs were filled with helium to the desired pressure. Then valve 2 was closed, and the pressure in the upstream reservoir was increased to the desired level
4. Valve 1 was closed and then valve 2 was opened. Driven by the pressure difference, the gas flowed from the upstream to the downstream side. The upstream and downstream pressure transients (P_u and P_d) were recorded by the transducers

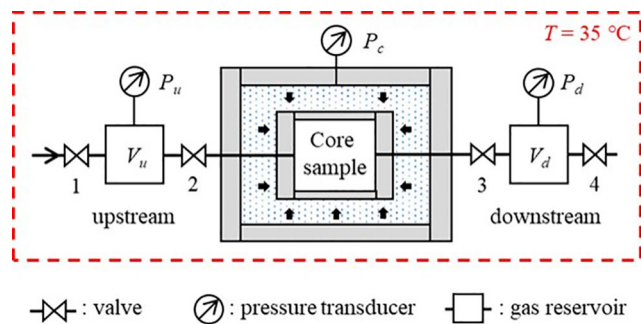


Figure 8. Scheme of the experimental setup.

The upstream pressure in the measurements varied from 0.90 to 1.75 MPa and the downstream pressure from 0.10 to 1.05 MPa. The porosity measured by He-pycnometry on the unstressed sample was 9.8%. Further information on the sample and the measurement is given in Table 1.

After the experiments, the recorded pressure transients were substituted into Equations 29 and 30 to evaluate the permeability coefficients. The apparent permeability deduced from one pulse-decay test is shown in Figure 9. The horizontal axis represents the time of the pressure recordings, and the vertical axis represents the permeability coefficients derived. At the early-time stage, the permeability values were nearly equal, though some small fluctuations caused by random errors were observed. The permeability values calculated from the early-time pressure records were averaged as the final result, which is marked by the dashed line in Figure 9. When using the pressure data beyond the early-time

Table 1
Parameters for the Pulse-Decay Tests

Core sample	Eagle Ford shale
Testing gas	Helium
Sample length L (m)	2.78×10^{-2}
Sample cross-section area A (m ²)	1.10×10^{-3}
Confining pressure P_c (MPa)	30, 40
Temperature T (°C)	35

stage, the permeability values show a clear deviation from the dashed line. Although the pulse-decay test shown here lasted for more than 1 hr (from applying a pressure pulse to a new pressure equilibrium), the permeability coefficient was obtained by the proposed method about 10 min after the start of the test, which proves that the proposed method is an efficient way to evaluate permeability.

The apparent permeability values calculated using the proposed approach and the late-time solution (Dicker and Smits' solution) (Dicker & Smits 1988) at different confining pressures and pore pressures are presented in Figure 10. The discrepancy between the permeability values calculated by the two models is less than 10%, which supports the viability of the proposed solution for reliable assessment of the permeability coefficients of tight rocks. Since the

proposed solution only needs the early-time data as input, it can give an estimate of the permeability coefficient in a short time. By combining the proposed early-time solution with the other late-time solutions (e.g., Dicker and Smits' solution), both the early-time and late-time pressure data can be interpreted, which helps to make full use of the information contained in the pulse-decay tests (Bhandari et al., 2015; Kamath et al., 1992).

5. Conclusions

In this study, an early-time solution was derived for the interpretation of pulse-decay measurements of tight rocks. The variations in gas compressibility and Klinkenberg slippage effects were considered in the derivation, resulting in a nonlinear diffusion equation for gas transport in porous media. The nonlinear equation was then solved approximately by an integral method, and an early-time solution was obtained. The proposed solution requires as input only the pressure recordings during the early-time stage of the pulse-decay tests, which makes it an efficient way of permeability evaluation and suitable for measurements on tight rocks. Helium is recommended as the testing fluid to minimize the influence of the Joule-Thomson effect and gas adsorption on pore walls. The numerical simulation was conducted to verify the proposed solution and determine the value of the parameters. Measurements under different confining pressures and pore pressures were performed on a core sample of the Cretaceous Eagle Ford shale, Texas, USA. The permeability values obtained by the proposed early-time solution and the late-time solution were in good agreement, which proves the accuracy of the proposed solution.

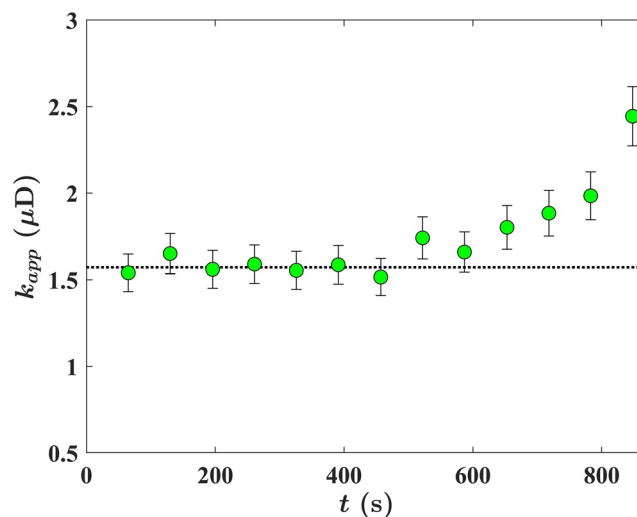


Figure 9. Interpretation of apparent permeability coefficients for the core sample in one pulse-decay test at 40 MPa confining pressure. The filled symbols represent the permeability values calculated from the pressure transient data at different instants, and the dashed line represents the average of the permeability coefficients calculated from the pressure recordings in the early-time stage (about 400 s in this test), above which the early-time solution becomes inapplicable as indicated by the increase of calculated permeability coefficient. The error bars account for the uncertainty in the pressure recording and the approximate error of setting $m/(n + 1) = 1.2$.

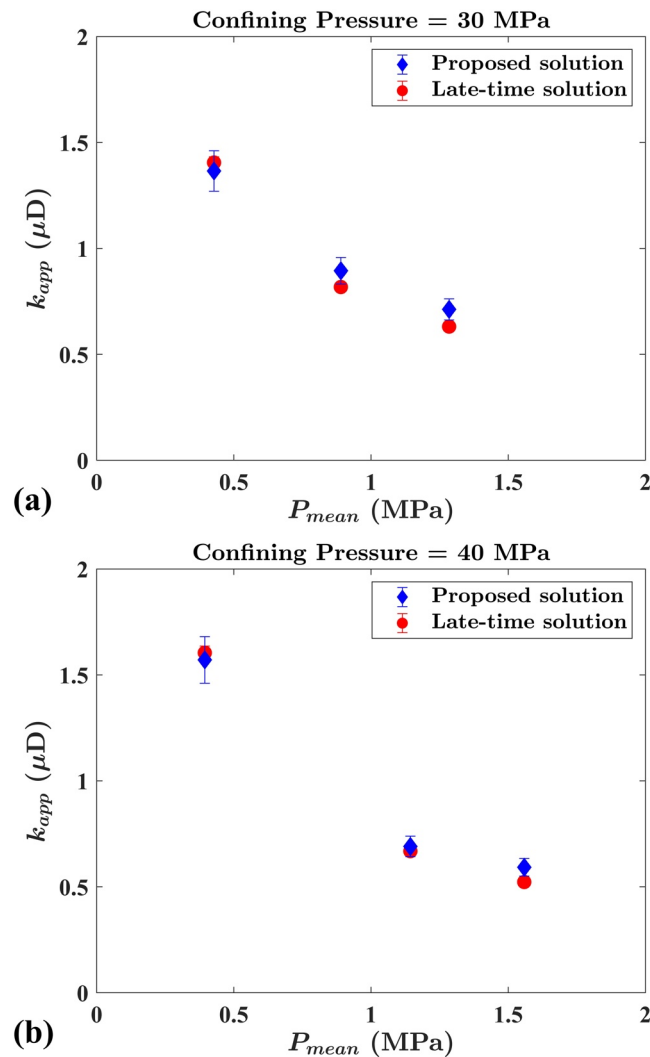


Figure 10. Apparent permeability coefficients calculated using the proposed solution (blue diamonds) and the late-time solution (Dicker & Smits, 1988; red circles) at confining pressures of 30 MPa (a) and 40 MPa (b), respectively.

Data Availability Statement

According to AGU's Data Policy, the data related to this article are placed into the community data repository. <http://doi.org/10.5281/zenodo.3541734>.

Acknowledgments

This work was financially supported by NSFC grants (Nos. U1837602, 11761131012) and the DFG grant AM 423/1-1 (Project number: 392108477; Joint Sino-German Research Project: Coupled Fluid Dynamic and Poro-Elastic Effects During Gas Flow in Nanoporous Media: Experiments and Multiscale Modeling "NanGasPor").

References

- Akkutlu, I. Y., & Fathi, E. (2012). Multiscale gas transport in shales with local kerogen heterogeneities. *SPE Journal*, 17(4), 1002–1011. <https://doi.org/10.2118/146422-PA>
- Bhandari, A. R., Flemings, P. B., Polito, P. J., Cronin, M. B., & Bryant, S. L. (2015). Anisotropy and stress dependence of permeability in the Barnett shale. *Transport in Porous Media*, 108(2), 393–411. <https://doi.org/10.1007/s11242-015-0482-0>
- Brace, W. F., Walsh, J. B., & Frangos, W. T. (1968). Permeability of granite under high pressure. *Journal of Geophysical Research*, 73(6), 2225–2236. <https://doi.org/10.1029/JB073i006p02225>
- Chalmers, G. R., Ross, D. J., & Bustin, R. M. (2012). Geological controls on matrix permeability of Devonian Gas Shales in the Horn River and Liard basins, northeastern British Columbia, Canada. *International Journal of Coal Geology*, 103, 120–131. <https://doi.org/10.1016/j.coal.2012.05.006>
- Cui, X., Bustin, A. M. M., & Bustin, R. M. (2009). Measurements of gas permeability and diffusivity of tight reservoir rocks: Different approaches and their applications. *Geofluids*, 9(3), 208–223. <https://doi.org/10.1111/j.1468-8123.2009.00244.x>
- Darabi, H., Etehad, A., Javadpour, F., & Sepehrnoori, K. (2012). Gas flow in ultra-tight shale strata. *Journal of Fluid Mechanics*, 710, 641–658. <https://doi.org/10.1017/jfm.2012.424>

- Dicker, A., & Smits, R. (1988). A practical approach for determining permeability from laboratory pressure-pulse decay measurement. In *Paper presented at International Meeting on Petroleum Engineering, Tianjin, China (SPE-17578-MS)*. Society of Petroleum Engineers. <https://doi.org/10.2118/17578-MS>
- Dong, J.-J., Hsu, J.-Y., Wu, W.-J., Shimamoto, T., Hung, J.-H., Yeh, E.-C., et al. (2010). Stress-dependence of the permeability and porosity of sandstone and shale from TCDP Hole-A. *International Journal of Rock Mechanics and Mining Sciences*, 47(7), 1141–1157. <https://doi.org/10.1016/j.ijrmms.2010.06.019>
- Fabre, A., & Hristov, J. (2016). On the integral-balance approach to the transient heat conduction with linearly temperature-dependent thermal diffusivity. *Heat and Mass Transfer*, 53(1), 177–204. <https://doi.org/10.1007/s00231-016-1806-5>
- Farcas, A., & Woods, A. W. (2007). On the extraction of gas from multilayered rock. *Journal of Fluid Mechanics*, 581, 79–95. <https://doi.org/10.1017/s0022112007005708>
- Fedor, F., Hámos, G., Jobbik, A., Máthé, Z., Somodi, G., & Szűcs, I. (2008). Laboratory pressure pulse decay permeability measurement of Boda Claystone, Mecsek Mts., SW Hungary. *Physics and Chemistry of the Earth, Parts A/B/C*, 33, S45–S53. <https://doi.org/10.1016/j.pce.2008.10.059>
- Feng, R., Harpalani, S., & Liu, J. (2017). Optimized pressure pulse-decay method for laboratory estimation of gas permeability of sorptive reservoirs: Part 2—Experimental study. *Fuel*, 191, 565–573. <https://doi.org/10.1016/j.fuel.2016.11.077>
- Feng, R., Liu, J., Chen, S., & Bryant, S. (2018). Effect of gas compressibility on permeability measurement in coalbed methane formations: Experimental investigation and flow modeling. *International Journal of Coal Geology*, 198, 144–155. <https://doi.org/10.1016/j.coal.2018.09.010>
- Feng, R., & Pandey, R. (2017). Investigation of various pressure transient techniques on permeability measurement of unconventional gas reservoirs. *Transport in Porous Media*, 120(3), 495–514. <https://doi.org/10.1007/s11242-017-0936-7>
- Fink, R., Krooss, B., & Amann-Hildenbrand, A. (2017). Stress-dependence of porosity and permeability of the Upper Jurassic Bossier shale: An experimental study. *Geological Society, London, Special Publications*, 454(1), 107–130. <https://doi.org/10.1144/sp454.2>
- Gaus, G., Amann-Hildenbrand, A., Krooss, B. M., & Fink, R. (2019). Gas permeability tests on core plugs from unconventional reservoir rocks under controlled stress: A comparison of different transient methods. *Journal of Natural Gas Science and Engineering*, 65, 224–236. <https://doi.org/10.1016/j.jngse.2019.03.003>
- Ghanizadeh, A., Gasparik, M., Amann-Hildenbrand, A., Gensterblum, Y., & Krooss, B. M. (2014). Experimental study of fluid transport processes in the matrix system of the European organic-rich shales: I. Scandinavian Alum Shale. *Marine and Petroleum Geology*, 51, 79–99. <https://doi.org/10.1016/j.marpetgeo.2013.10.013>
- Goodman, T. R. (1958). The heat balance integral and its application to problems involving change of phase. *Transactions of the ASME Journal of Heat Transfer*, 80, 335.
- Hahn, D. W., & Özisik, M. N. (2012). *Heat conduction*. John Wiley & Sons.
- Han, G., Sun, L., Liu, Y., & Zhou, S. (2018). Analysis method of pulse decay tests for dual-porosity cores. *Journal of Natural Gas Science and Engineering*, 59, 274–286. <https://doi.org/10.1016/j.jngse.2018.09.006>
- Hannon, M. J., Jr. (2020). *Fast and accurate core analysis by the full-immersion pressure-pulse decay: Part 2—Practice and demonstration*. SPE Reservoir Evaluation & Engineering.
- Heller, R., & Zoback, M. (2013). Laboratory measurements of matrix permeability and slippage enhanced permeability in gas shales. In *Paper presented at Unconventional Resources Technology Conference*. Society of Exploration Geophysicists, American Association of Petroleum.
- Hsieh, P., Tracy, J., Neuzil, C., Bredehoeft, J., & Silliman, S. E. (1981). A transient laboratory method for determining the hydraulic properties of ‘tight’ rocks—I. Theory. *International Journal of Rock Mechanics and Mining Sciences & Geomechanics Abstracts*, 18(3), 245–252.
- Jia, B., Jin, L., Mibeck, B. A., Smith, S. A., & Sorensen, J. A. (2020). An integrated approach of measuring permeability of naturally fractured shale. *Journal of Petroleum Science and Engineering*, 186, 106716. <https://doi.org/10.1016/j.petrol.2019.106716>
- Jones, S. C. (1997). A technique for faster pulse-decay permeability measurements in tight rocks. *SPE Formation Evaluation*, 12(1), 19–26. <https://doi.org/10.2118/28450-Pa>
- Kamath, J., Boyer, R., & Nakagawa, F. (1992). Characterization of core scale heterogeneities using laboratory pressure transients. *SPE Formation Evaluation*, 7(3), 219–227. <https://doi.org/10.2118/20575-PA>
- Klinkenberg, L. (1941). The permeability of porous media to liquids and gases. In *Paper presented at Drilling and production practice*. OnePetro.
- Liang, Y., Price, J. D., Wark, D. A., & Watson, E. B. (2001). Nonlinear pressure diffusion in a porous medium: Approximate solutions with applications to permeability measurements using transient pulse decay method. *Journal of Geophysical Research*, 106(B1), 529–535. <https://doi.org/10.1029/2000JB900344>
- Liu, P., Ju, Y., Gao, F., Ranjith, P. G., & Zhang, Q. (2018). CT identification and fractal characterization of 3-D propagation and distribution of hydrofracturing cracks in low-permeability heterogeneous rocks. *Journal of Geophysical Research: Solid Earth*, 123, 2156–2173. <https://doi.org/10.1002/2017JB015048>
- McCarty, R. D., & Arp, V. D. (1990). A new wide range equation of state for helium. In *Advances in cryogenic engineering* (pp. 1465–1475). Springer.
- Metwally, Y. M., & Sondergeld, C. H. (2011). Measuring low permeabilities of gas-sands and shales using a pressure transmission technique. *International Journal of Rock Mechanics and Mining Sciences*, 48(7), 1135–1144. <https://doi.org/10.1016/j.ijrmms.2011.08.004>
- Mitchell, S. L., & Myers, T. G. (2010). Improving the accuracy of heat balance integral methods applied to thermal problems with time dependent boundary conditions. *International Journal of Heat and Mass Transfer*, 53(17–18), 3540–3551. <https://doi.org/10.1016/j.jheatmasstransfer.2010.04.015>
- Nolte, S., Fink, R., Krooss, B. M., Amann-Hildenbrand, A., Wang, Y., Wang, M., et al. (2021). Experimental investigation of gas dynamic effects using nanoporous synthetic materials as tight rock analogues. *Transport in Porous Media*, 137, 519–553. <https://doi.org/10.1007/s11242-021-01572->
- Özışık, M. N. (1989). *Boundary value problems of heat conduction*. Courier Corporation.
- Richtmyer, R. D., & Morton, K. W. (1994). Difference methods for initial-value problems. *SIAM Review*, 10(3), 381–383. <https://doi.org/10.1137/1010073>
- Sander, R., Pan, Z., & Connell, L. D. (2017). Laboratory measurement of low permeability unconventional gas reservoir rocks: A review of experimental methods. *Journal of Natural Gas Science and Engineering*, 37, 248–279. <https://doi.org/10.1016/j.jngse.2016.11.041>
- Schlichting, H., & Gersten, K. (2016). *Boundary-layer theory*. Springer.
- Senger, R., Romero, E., & Marschall, P. (2018). Modeling of gas migration through low-permeability clay rock using information on pressure and deformation from fast air injection tests. *Transport in Porous Media*, 123(3), 563–579. <https://doi.org/10.1007/s11242-017-0962-5>
- Sun, Z., Zhou, S., Li, J., Chen, K., Zhang, C., Zhang, Y., & Li, P. (2020). Laboratory research on gas transport in shale nanopores considering the stress effect and slippage effect. *Journal of Geophysical Research: Solid Earth*, 125, e2019JB018256. <https://doi.org/10.1029/2019JB018256>

- Wang, Y., Liu, S., & Elsworth, D. (2015). Laboratory investigations of gas flow behaviors in tight anthracite and evaluation of different pulse-decay methods on permeability estimation. *International Journal of Coal Geology*, *149*, 118–128. <https://doi.org/10.1016/j.coal.2015.07.009>
- Wang, Z., Fink, R., Wang, Y., Amann-Hildenbrand, A., Krooss, B. M., & Wang, M. (2018). Gas permeability calculation of tight rocks based on laboratory measurements with non-ideal gas slippage and poroelastic effects considered. *International Journal of Rock Mechanics and Mining Sciences*, *112*, 16–24. <https://doi.org/10.1016/j.ijrmms.2018.10.002>
- Winhausen, L., Amann-Hildenbrand, A., Fink, R., Jalali, M., Khaledi, K., Hamdi, P., et al. (2021). A comparative study on methods for determining the hydraulic properties of a clay shale. *Geophysical Journal International*, *224*(3), 1523–1539.
- Wu, T., Pan, Z., Connell, L. D., Camilleri, M., & Fu, X. (2020). Apparent gas permeability behaviour in the near critical region for real gases. *Journal of Natural Gas Science and Engineering*, *77*, 103245. <https://doi.org/10.1016/j.jngse.2020.103245>
- Yang, Z., Dong, M., Zhang, S., Gong, H., Li, Y., & Long, F. (2016). A method for determining transverse permeability of tight reservoir cores by radial pressure pulse decay measurement. *Journal of Geophysical Research: Solid Earth*, *121*, 7054–7070. <https://doi.org/10.1002/2016JB013173>
- Zhao, J., Kang, Q., Wang, Y., Yao, J., Zhang, L., & Yang, Y. (2020). Viscous dissipation and apparent permeability of gas flow in nanoporous media. *Journal of Geophysical Research: Solid Earth*, *125*, e2019JB018667. <https://doi.org/10.1029/2019JB018667>